GEOPHYSICS. VOL. 77, NO. 1 (JANUARY-FEBRUARY 2012); P. B1–B10, 13 FIGS., 1 TABLE.
10.1190/GEO2011-0074.1

Robust prestack *Q*-determination using surface seismic data: Part 2 — 3D case study

Carl Reine[1], Roger Clark[2], and Mirko van der Baan[3]

ABSTRACT

In part one of this paper, we introduced a novel method of measuring seismic attenuation from prestack surface seismic data. This prestack Q-inversion (PSQI) employed methods to reduce the presence of spectral interference and then minimize the influence of interference that remains. By changing the domain of operation, angle-dependent effects in the overburden were eliminated when a locally 1D medium was assumed. To demonstrate the suitability of the PSQI method, we applied it to a 3D seismic survey from Western Canada. Preprocessing of the data was carried out to reduce noise, regularize amplitudes, and transform the seismic gathers into the τ-p domain prior to attenuation measurements. In addition to the seismic gathers, we also incorporated velocity data and zero-offset traveltime information. The result was that we were able to generate a map of 1/Q values which showed coherent patterns that could be explained by the presence of top gas in the reservoir. These measurements were correlated to independent amplitude attributes. We performed a number of other analyses to establish the appropriateness of the attenuation measurements. We compared 1/Q measurements with the predecessor QVO method, and showed that the PSQI measurements were less influenced by artifacts and were more robust to changes in the bandwidth of analysis. We also analyzed a VSP survey in the same geological setting and showed that the resulting measurement (1/Q = 0.0271) is very close to the mean PSQI value for the 3D survey (1/Q = 0.0312). This case study thus showed how the described PSQI method overcame many of the difficulties associated with obtaining accurate attenuation measurements from surface seismic data.

INTRODUCTION

Resolution of a seismic wave decreases as it travels through an attenuating medium, and the associated dispersion alters the phase spectrum. Knowledge of attenuation, through the quality factor Q, can thus be used to compensate for these effects and improve the resolution of the data (Wang, 2002). Additionally, the magnitude of the attenuation is directly related to petrophysical parameters, such as gas saturation (Winkler and Nur, 1982) or heavy-oil viscosity (Behura et al., 2007), thus providing a potential tool for reservoir characterization. To extract this valuable information, a reliable means of measuring attenuation must be used.

In part one of this paper (Reine et al., this issue), we introduced a robust method (referred to as prestack Q-inversion, PSQI) for measuring effective interval attenuation from surface seismic data, which minimizes corrupting factors such as spectral interference and angle-dependent effects in the overburden. This was achieved through three main components of the method: using variable-window time-frequency transforms for spectral measurements; using an inversion scheme which deals simultaneously with all of the prestack common midpoint (CMP) data in both the frequency and traveltime-difference coordinates, and which can be weighted to favor those frequencies and traveltime differences considered most robust; and by operating along traces of constant horizontal slowness through the use of the τ-p transform under an assumption of a 1D medium.

Here, we demonstrate the PSQI method in a case study using CMP data from a shallow 3D land-seismic survey from the Alberta

Manuscript received by the Editor 18 February 2011; revised manuscript received 5 September 2011; published online 3 February 2012; corrected version published online 9 February 2012.
[1]Formerly University of Leeds, School of Earth and Environment, Leeds, U. K.; presently Nexen Inc., Calgary, Alberta, Canada. E-mail: carl_reine@nexeninc.com.
[2]University of Leeds, School of Earth and Environment, Leeds, U. K. E-mail: r.clark@see.leeds.ac.uk.
[3]University of Alberta, Department of Physics, Edmonton, Alberta, Canada. E-mail: mirko.vanderbaan@ualberta.ca.

oil sands. We first calculate maps of $1/Q$ for a zone in which one of the bounding reflections is heavily influenced by tuning. This exercise demonstrates the decreased sensitivity of the PSQI method to interference effects compared to the QVO method of Dasgupta and Clark (1998). We then calculate $1/Q$ for an interval encompassing the reservoir, and show that the PSQI-measured $1/Q$ values offer improved stability to those obtained with the QVO method. Furthermore, we compare the measured attenuation with the stacked amplitude of a reservoir-level reflection, which corresponds to the top of gas accumulation in the reservoir. This comparison offers a possible petrophysical explanation of the attenuation results, and demonstrates that the PSQI method can adequately measure attenuation values suitable for interpretation purposes. Finally, to show that the PSQI-measured attenuation has appropriate magnitude, we compare these measurements to $1/Q$ obtained from a nearby vertical seismic profile (VSP) in the same geological setting.

BACKGROUND AND THEORY

Geological background

The reservoir investigated by this data set is the McMurray sandstone (Figure 1), described in detail by the AEUB (2003). As a large-scale channel deposit, its morphology is determined by the paleotopography of the underlying Devonian carbonates. The McMurray formation is an unconsolidated sandstone, characterized by porosities of 30% or greater. Because the formation is poorly consolidated, and because of the high viscosity of the oil ($\geq 100\,\mathrm{Pa}\cdot\mathrm{s}$), the matrix is partially cemented by heavy oil (Macrides and Kanasewich, 1987). This presents unique mechanisms for seismic attenuation where the heavy oil itself supports viscous relaxation (Behura et al., 2007). The overburden consists of alternating sandstone and mudstone layers. The formation immediately overlying the McMurray is the Clearwater, the lower portions of which constitute the Wabiskaw member.

The main production from the McMurray reservoir is of heavy oil, or bitumen, with an API gravity less than 15°. Generally, the bitumen overlies a water zone, and may also have associated top gas or gassy water (AEUB, 2003). The location of this gas is frequently correlated with the presence of channel deposits near the top of the reservoir, although this is not a requirement for gas accumulation. Because of the differences in attenuation mechanisms between the heavy oil and of gas, attenuation is potentially a useful tool for discriminating between these two fluid types. The fact that the presence of gas in the reservoir lowers significantly the seismic impedance also allows for the reflection amplitude to be used to support the presence of these gas accumulations.

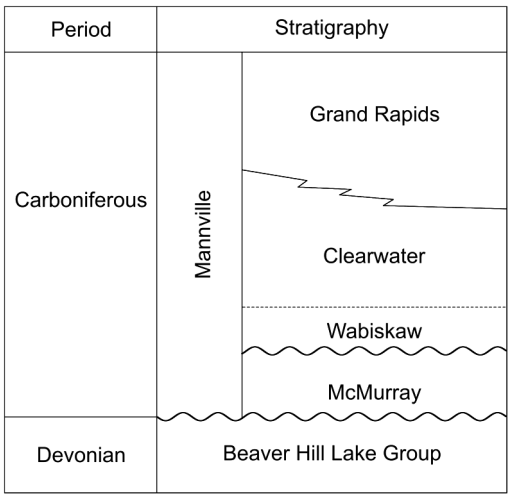

Figure 1. The relevant geological formations of the Alberta oil sands. Based on Wightman and Pemberton (1997).

Survey parameters

The 3D survey acquisition parameters were designed to image the shallow (<400 ms) reservoir using point sources and point receivers. A dense surface grid of explosives and multicomponent digital receivers was deployed, resulting in a natural bin size of 10×10 m. The number of recorded channels for each shot results in a fold of approximately 90. Although thermal recovery is required for field development, the survey was acquired before the injection of steam.

The CMP data that we use form a rectangular subset of the entire survey, 284 inlines by 327 crosslines in size. On the north edge of the survey around crossline 210 (crossline 70 for 30 m superbins), there is an area of poor data quality caused by the presence of a lake. This feature affects the data quality, which in turn corrupts the attenuation and amplitude measurements. Although the region clearly expresses itself in the mapped values, it is also outlined on all mapped results.

A VSP survey is also available for attenuation analysis. The VSP is not within the area bounded by the subset of surface seismic data, but is from a nearby field with similar geology. The well in which the VSP was acquired does not have any gas present in the reservoir. The VSP is recorded with 66 receivers ranging in depth from surface to 498 m. The data are acquired using explosives in two shots, each with the receiver cable spanning the entire depth range, but the position of the receivers are interleaved between shots. The source offsets are 26 and 27 m for the two shots, providing near-vertical incidence angles for the direct and reflected waves.

The PSQI method

The components of the prestack Q-inversion approach and their justification are described in Part 1 of this paper. Figure 2 shows a flow diagram of the PSQI method, and in this section, we summarize these components for convenience. An expansion of the specific details as they pertain to nonsynthetic data is reserved for the following section.

The prestack CMP gathers are most effectively analyzed in the τ-p domain, where a laterally homogeneous velocity and attenuation structure are assumed. In this domain, traces of constant horizontal slowness are analyzed, which allows a cancellation of angle-dependent effects in the overburden, such as source or receiver directivity or attenuation anisotropy. Moveout curves for the reflections bounding the interval of interest may be defined in the τ-p domain with the knowledge of the stacking velocity field and zero-offset times of interest (Part 1, equations 8 and 9). This allows the appropriate spectra to be extracted from the time-frequency representation of each trace, obtained by using the S-transform (Stockwell et al., 1996).

The spectra from the bounding reflections are then used to calculate a natural log spectral ratio for each trace (Part 1, equation 4).

This collection of natural log spectral ratios for a single CMP is then inverted simultaneously to directly obtain an interval $1/Q$ (Part 1, equation 16). The traveltime differences needed for this inversion are obtained using the equivalent traveltimes for the τ-p domain data (Part 1, equation 12). This inversion may also be weighted to reduce the influence of unpredictable elements in the data. These weights are calculated using multiple realizations of the data, and are such that they vary for each frequency and traveltime-difference considered (Part 1, equation 20).

The QVO Method

The PSQI method is described in part one of this paper, but here we review the QVO method introduced by Dasgupta and Clark (1998) as a comparison tool in this study. The QVO method was an early attempt at measuring effective attenuation from t-x domain CMP data, taking statistical advantage of the prestack fold. The effectiveness of QVO has been demonstrated in a number of applications, including discrimination of lithology types (Dasgupta and Clark, 1998; Hackert and Parra, 2004), azimuthal discrimination of fractures (Clark et al., 2009; Moffat et al., 2009), and time-lapse changes (Clark et al., 2001; Blanchard et al., 2009). Along with the successes, however, the QVO method has also been shown to be sensitive to corrupting influences such as spectral interference from tuning and intrabed multiples (Carter, 2003).

We use two adaptations to the QVO method to compare it more fairly to the PSQI method. First, we follow Guerrero Moreno (2007) in using CMP gathers that have not been NMO corrected, avoiding NMO stretch effects, and second we adopt a development of Carter (2003) that avoids the need for a parabolic traveltime approximation. The QVO process can then be broken down into the general steps of spectral estimation and inversion for $1/Q$.

The spectrum $S_1(f)$ of a chosen reflection is first estimated for each trace, resulting in a spectrum for every CMP offset. In the QVO method this is done with a windowed Fourier transform. The natural log spectral ratio of each spectrum is then taken with respect to the measured source spectrum or that of a strong, shallow, near-offset event $S_0(f)$:

$$\ln\left[\frac{S_1(f)}{S_0(f)}\right] = -\frac{\pi}{Q}\Delta t f + \ln(PG), \tag{1}$$

where Δt is the time difference between the reference and measured events, and the terms P and G refer to the amplitude effects of energy partitioning and geometric spreading, respectively.

The QVO approach for inversion of $1/Q$ involves two independent inversions. In the first step, a linear regression of the natural log spectral ratio with respect to frequency f yields a collection of individual slopes at each trace:

$$A = -\frac{\pi\Delta t}{Q}. \tag{2}$$

Because the traveltime difference Δt experienced by each offset is different, a second inversion of the equation

$$A = A'\Delta t + B' \tag{3}$$

may then be used, where

$$A' = -\frac{\pi}{Q}, \tag{4}$$

and B' is expected to be zero. This second inversion is weighted by the uncertainty in the slope calculation of the first inversion. The result is that the zero-offset slope $A(t_0)$, and hence, $1/Q$ is determined. Interval values of $1/Q$ are finally obtained from appropriate differencing of the traveltime weighted average measurements.

SEISMIC DATA ANALYSIS

We choose two intervals for our attenuation analysis. The upper limit of both intervals is a strong seismic reflection just below the top of the Clearwater formation. The first interval, in which intrinsic attenuation is expected to be relatively uniform, is bounded below by the top of the McMurray reservoir. This lower limit is heavily influenced by tuning, and is chosen to demonstrate the impact that this interference has on each of the measurements. The second interval includes the McMurray reservoir, using the reflection from the Devonian carbonate as its lower limit. This interval is expected to see the changes in attenuation caused by top gas, without being influenced by the tuned McMurray reflection. The attenuation values that we present are interval values between the upper and lower limits of each zone.

Preprocessing

The preprocessing required for attenuation measurements is not necessarily the same as that used to obtain an optimal stacked image. Processes such as deconvolution strongly affect the spectrum of the data, and are therefore avoided. Similarly, processes

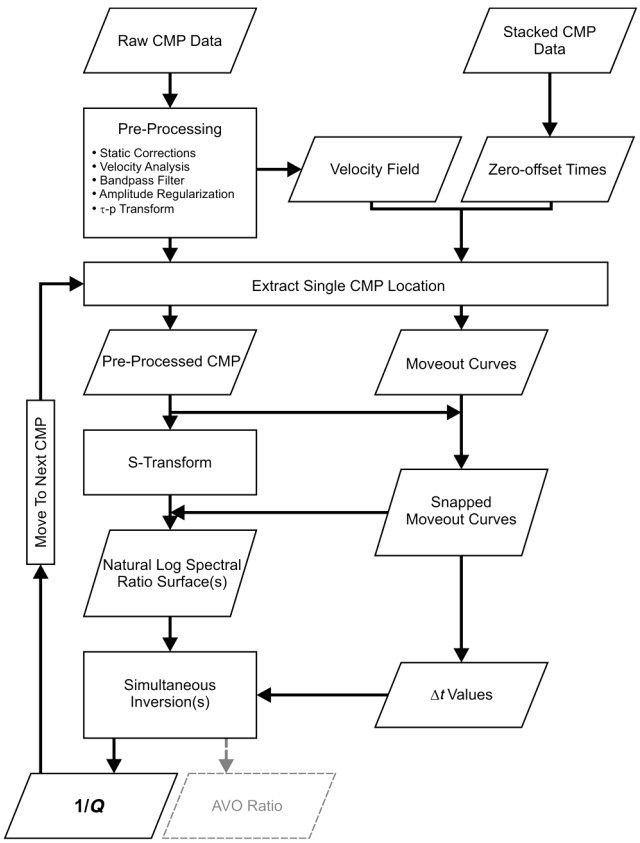

Figure 2. Flow diagram of the PSQI method. CMP data as well as processing velocities and interpretation from stacked data are used as inputs to arrive at a map of $1/Q$ values.

such as *f-k* filtering that have the potential to introduce artifacts into the spectrum of the data are likewise omitted. To optimize the PSQI analysis, processing is limited to the steps described here.

The data were received with static corrections and velocity analysis already performed. We first use a 12-24-120-180-Hz Ormsby band-pass filter to exclude completely the surface-wave energy below its peak frequency of 10 Hz. The high end of the filter corresponds to the limits of the seismic spectrum.

Trace amplitude corrections are next calculated in a surface-consistent manner (Taner and Koehler, 1981). Before these calculations, excessively noisy traces are eliminated manually from the data, and geometric spreading corrections (Ursin, 1990) are applied to prevent bias in the offset component. The shot, receiver, and channel amplitude corrections are then applied to data without geometric spreading compensation.

Before the τ-p transform is applied, steps must be taken to reduce truncation artifacts and aliasing. The direct wave is removed with a top mute, and to reduce the strength of far-offset truncation artifacts, we apply a linear far-offset taper over the final third of the traces. To minimize transform aliasing, the offset distribution is improved by rebinning the data to form 3×3 superbins.

The upper limit of horizontal slownesses (1 ms/m) for the τ-p transform exceeds the largest slowness of the shallow reflections, and provides a buffer zone of high slownesses beyond this point. The minimum transform slowness is the negative of the maximum slowness, and the traces corresponding to the negative horizontal slownesses are truncated following the transform. We calculate a total of 901 positive slownesses, which is the approximate fold of the CMP supergather. A final preprocessed CMP in the τ-p domain is shown in Figure 3, and the three reflections considered are indicated.

As described in part one, this implementation of the τ-p transform is suitable for 2D space, however, because the data do not match this condition, nor are line sources used, the transformed amplitudes are partially affected by geometric spreading (van der Baan, 2004). While this will not affect the $1/Q$ results, it must be considered if the intercept terms are to be used for AVO analysis, as described in Part 1 of this paper.

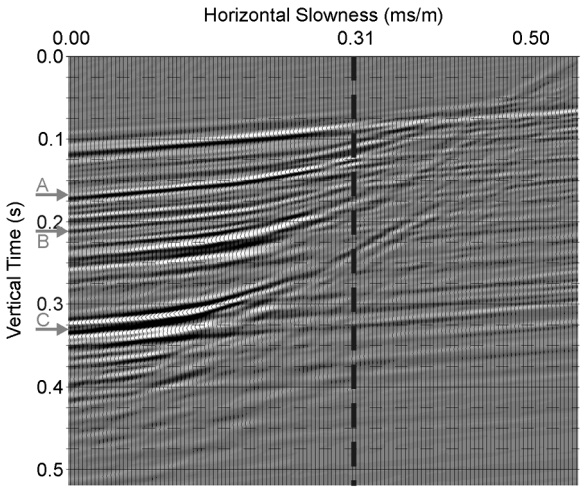

Figure 3. A final preprocessed CMP gather in the τ-p domain. The Clearwater, McMurray, and Devonian reflections are indicated (A, B, and C, respectively). The maximum horizontal slowness present in the data for the Devonian reflection is also shown, corresponding to the limit of the trace analysis.

Stacked data analysis

For both the PSQI and QVO methods, zero-offset times are required to calculate the relevant moveout curves. To obtain the zero-offset times, the data are stacked in the t-x domain following the surface-consistent amplitude corrections. These stacked data, as well as the velocity field, are referenced to the same datum as the gathers being analyzed. Horizons of interest are then interpreted based on well-log ties, yielding the necessary zero-offset times for each CMP.

A stacked inline from the 3D volume and the reflections of importance, as determined from a synthetic tie, are shown in Figure 4. The middle horizon indicated corresponds to the top of the McMurray reservoir. This zone is encompassed by the top and bottom horizons, the Clearwater and Devonian, respectively. These three reflections are used for the interval attenuation analysis.

The stacked data are also useful for identifying gas near the top of the McMurray reservoir. As well as being a potential attenuation mechanism, the presence of top gas within the reservoir causes a decrease in the P-wave impedance relative to the gas-free case. As introduced in the geological background, this gas is expected to have a laterally variable distribution.

The negative impedance contrast caused by the stratigraphically trapped gas results in a strong negative reflection just below the top reflection. We extract the minimum stacked amplitude from within 20 ms below the top of the McMurray to capture this reflection character (Figure 5). In the mapped values, a strong negative amplitude response is evident in the center of the survey, which shows sharp lateral boundaries due to stratigraphic changes. A number of features are identified for comparison with the attenuation results.

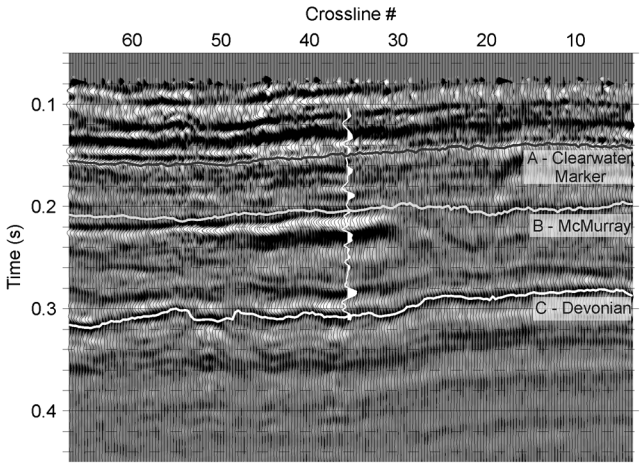

Figure 4. Inline 40 stacked following the preprocessing applied for attenuation measurements, excluding those processes related to the τ-p transform. Inline and crossline values refer to 30-m superbin centers for comparison with the maps. Three horizons of relevance are shown: the tops of the Clearwater, Devonian, and McMurray reservoir. The high negative amplitude response below the McMurray near crossline 35 is indicative of top gas. The synthetic tie is also shown.

PSQI Analysis

In addition to the prepared τ-p domain gathers, the interval velocity field and zero-offset times are required to describe the τ-p moveout curves of the bounding reflections (Part 1, equation 8). Zero-offset times are determined from the stacked data as described above, and the velocity field is determined through velocity analysis. We convert these stacking velocities to interval values using Dix's equation (Dix, 1955).

Often, the calculated moveout curves in either the t-x or τ-p domains do not match exactly the arrival time of the reflected seismic energy. This is due to a number of factors, including higher-order moveout, the use of isotropic velocities in the presence of anisotropy, lateral inhomogeneity in the velocity field, the presence of body-wave dispersion, and in the t-x domain, statics errors. In the absence of information to account for these possibilities, Guerrero Moreno (2007) hand picks the moveout of each trace individually for t-x domain QVO analysis. This is a time consuming process however, which becomes prohibitive for large data volumes. To automate this process on our τ-p gathers, we search within a threshold window of the theoretical moveout curves to find the maximum amplitude of the envelope of the analytical signal (Taner et al., 1979). By adjusting the moveout curve, this step helps to compensate for errors in the velocity assumptions or time picks. The equivalent traveltimes are then updated following this moveout adjustment (Part 1, equation 12).

The S-transform of a τ-p domain CMP gather is taken to produce a time-frequency representation for each trace (Reine et al., 2009). Traces that approach the horizontal slowness of refraction or those that exceed the horizontal slownesses present in the t-x data are omitted from the analysis. Individual spectra from the three bounding reflections are then extracted for each horizontal slowness trace from the appropriate sample location determined by the adjusted moveout curve (refer to Figure 2).

After the necessary spectra are extracted, the natural log spectral ratio surface is calculated for each interval. These surfaces are inverted, in this case using a primary bandwidth of 25 to 150 Hz (Reine, 2009), and the $1/Q$ value and its uncertainty are calculated for the CMP. The calculations are repeated using additional bandwidths of 25 to 125 Hz, and 40 to 150 Hz. To reduce the influence of noisy frequencies and spectral interference, we use a weighting function in the inversion (Part 1, equation 20). We achieve this in a spatial sense by grouping adjacent CMPs together into a rolling 3×3 superbin. The mean of the natural log spectral ratios is used as the inversion input, and the inverse of the variance at each individual frequency is used as the weight. In this manner, noisy frequencies are inherently down weighted. The spatial weighting approach works particularly well for our τ-p transformed data, for which the horizontal slownesses present in each gather are the same. This ensures that the data may be combined easily over the traveltime-difference coordinate.

For the larger Clearwater to Devonian interval, the mean natural log spectral ratio surface from one CMP is shown in Figure 6a. This surface displays the characteristics expected according to the spectral ratio equation (Part 1, equation 4), namely that the ratio decreases in value as either frequency or traveltime difference increases. Figure 6b shows the inverted solution to the surface in Figure 6a. The solution is linear in the frequency coordinate, and indeed the traveltime-difference coordinate as well, once the frequency-independent, trace-to-trace amplitude shift is accounted for. This amplitude shift (Part 1, equation 18) contains the amplitude

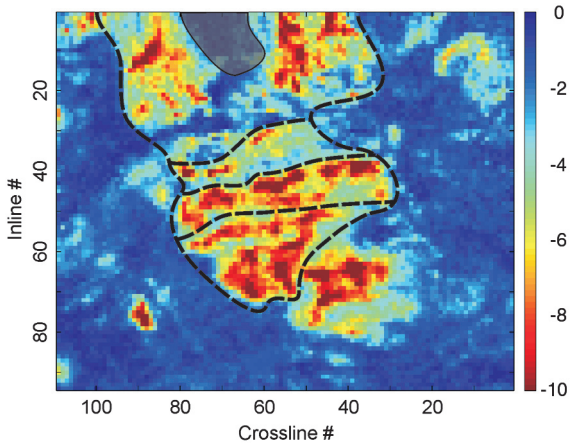

Figure 5. Minimum stacked amplitude within a zone 20 ms below the McMurray horizon. The amplitude scale has been normalized. The strong negative response (red) corresponds to the presence of top gas in the reservoir. These effects are also seen in Figure 4. The boundary of the amplitude response and various features are identified for comparison with the $1/Q$ results. The area of poor data quality below a lake is greyed out.

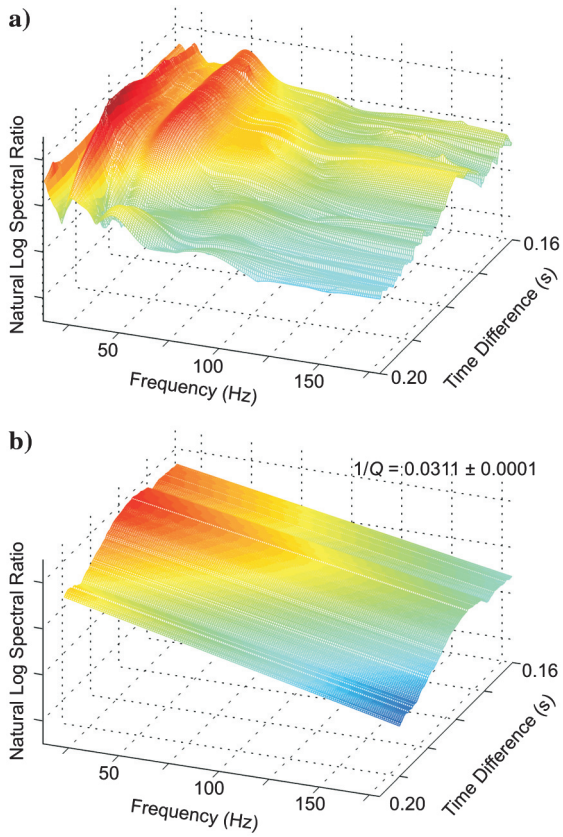

Figure 6. (a) The mean natural log spectral ratio surface for a single superbin location. The ratio decreases as expected with an increase along either the frequency or time difference axis. The solution surface to this input data (b) allows for a trace-to-trace amplitude shift, resulting in a folded appearance.

components which vary by trace, such as residual geometric spreading and energy partitioning effects, and appears as "folds" in the surface.

QVO Analysis

The same data are analyzed using the QVO method described above to provide a comparison with the PSQI results. Because the gathers remain in the *t-x* domain for QVO analysis, the preprocessing stops after the application of surface-consistent amplitude scaling. The *t-x* moveout curves are calculated using the zero-offset times and stacking velocities as before. Similar to the PSQI measurements, these curves are snapped to the maximum of the instantaneous amplitude to account for residual statics errors and the other effects previously discussed.

Spectral estimates are performed with a windowed Fourier transform using a Hamming taper. The average $1/Q$ is calculated to both the upper $(1/Q_1)$ and lower $(1/Q_2)$ reflections that bound the interval being analyzed. We then obtain an interval $1/Q_{12}$ by subtracting these averages weighted by the respective traveltimes t_1 and t_2:

$$\frac{1}{Q_{12}} = \frac{1}{t_{12}}\left(\frac{t_2}{Q_2} - \frac{t_1}{Q_1}\right). \tag{5}$$

Here, t_{12} is the difference in traveltimes t_1 and t_2. The primary inversion bandwidth is the same as that used for the PSQI measurements (25 to 150 Hz), and the calculations using the two additional bandwidths (25 to 125 Hz and 40 to 150 Hz) are also performed. The weighting for the second inversion to obtain $1/Q$ is determined by the uncertainty of the individually inverted slopes from the first inversion.

VSP analysis

We finally analyze the attenuation in the Clearwater to Devonian interval using VSP data as an independent attenuation measurement for the geology considered. Although the VSP is not in the same immediate survey area as the surface seismic, it is in the same geological setting acquired in a well without gas in the McMurray. This analysis looks to confirm independently that the PSQI-calculated $1/Q$ values are reasonable.

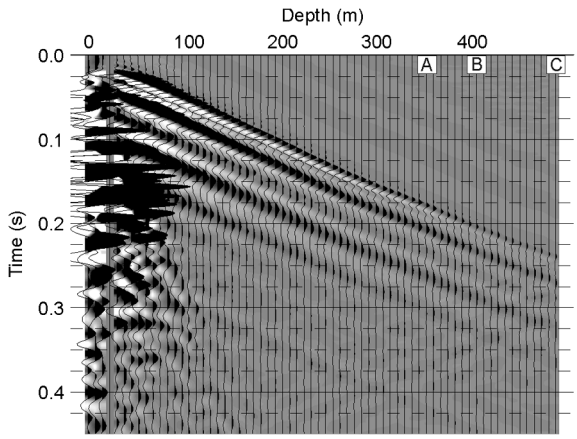

Figure 7. Preprocessed downgoing wavefield of the VSP survey. The depths of the three horizons shown in Figure 4 are indicated (A, Clearwater; B, McMurray; C, Devonian).

The VSP data are first preprocessed to make them suitable for attenuation analysis. The downgoing wavefield is isolated by applying a three-point median filter following alignment on the first arrivals. A band-pass filter is also applied with the same corner frequencies as those applied to the surface seismic data. This eliminates high- and low-frequency noise, and regularizes the frequency range of the two experiments. Figure 7 shows the preprocessed downgoing wavefield. The depths of the three interfaces shown in Figure 4 are indicated, and it can be seen that very little upgoing energy remains near the direct wave.

To measure attenuation, it is conventional to use the spectral ratio method between the direct wave of a single upper and lower trace pair. As with the PSQI measurements, the inversion bandwidth is set at 25 to 150 Hz. Using the receivers closest to the geological boundaries, the measured attenuation for the interval is $1/Q = 0.033 \pm 0.003$.

Single measurements, as in the surface seismic case, are potentially dominated by interference effects, resulting in anomalous spectral ratios. To improve the stability of the VSP attenuation measurements, we assume that the bounding interval has a homogeneous $1/Q$, and we analyze all receiver-pair combinations within this zone. Although this analysis could be done with each pair individually, the simultaneous inversion scheme introduced here (Part 1, equation 16) is a more appropriate approach. In the VSP case, the natural log spectral ratio surface is arranged such that the time difference coordinate of the inversion corresponds to the difference in downgoing-wave arrival times for a given receiver-pair. The calculation of attenuation from this type of inversion yields a $1/Q = 0.0271 \pm 0.0002$.

RESULTS

The results for the upper interval, bounded by the Clearwater and McMurray reflections, are useful to demonstrate how tuning interference from the strong top-gas reflection influences the attenuation measurements. Figure 8 shows in plan view the $1/Q$ values calculated for all CMPs in the survey for both the PSQI and QVO methods using the primary bandwidth. Both maps show an obvious similarity to the amplitude map (Figure 5), with an area of high attenuation measured in the center of the survey. Because this interval is not expected to see intrinsic attenuation effects from the top gas, which falls below the base of the interval, the high attenuation measured in the center is most likely apparent attenuation caused by tuning. The magnitude of this effect is much greater for the QVO measurements than for the PSQI values, indicating that PSQI is less influenced by interference effects.

Whereas the upper interval is influenced by tuning at the McMurray reflection, the larger Clearwater to Devonian interval is independent of this reflection. Figure 9 shows the $1/Q$ values calculated for this zone derived from both methods using the primary bandwidth. There is an area of higher attenuation in the center of the survey, and within this area there are a number of spatially coherent features identified that are similar to those shown on the amplitude map (Figure 5). While a number of features in the QVO results are similar to those using PSQI, there are other features imprinted as well. Specifically, these imprinted features on the QVO results relate to the isochron between the two reflections analyzed (Figure 10). The cause of this is discussed further below.

Changing the inversion bandwidths of the PSQI and QVO measurements shows the relative stabilities of the methods, because frequency-independent Q measurements should be independent of the bandwidth in the absence of influence from corrupting factors. Figure 11 shows the $1/Q$ values for both methods using the bandwidth of 40 to 150 Hz. The magnitudes of the PSQI values are more similar to the values calculated with the primary bandwidth than are the QVO values (Figure 9). Specifically, the QVO results show a significant increase in the measured attenuation across the data arising from the bandwidth change.

The effects of bandwidth stability can also be investigated from a statistical standpoint. With respect to the measurements using the original bandwidth, the median value of the PSQI measurements shows an 11% increase and the median of the QVO measurements decreases by 19% when the bandwidth is changed to 25 to 125 Hz (Figure 12a and 12b). This is a 1.7 times greater shift for the QVO results. Similarly, when the bandwidth is changed to 40 to 150 Hz, the median shift for the PSQI results is an increase of 6%, whereas the QVO results increase by 21%, or 3.5 times as

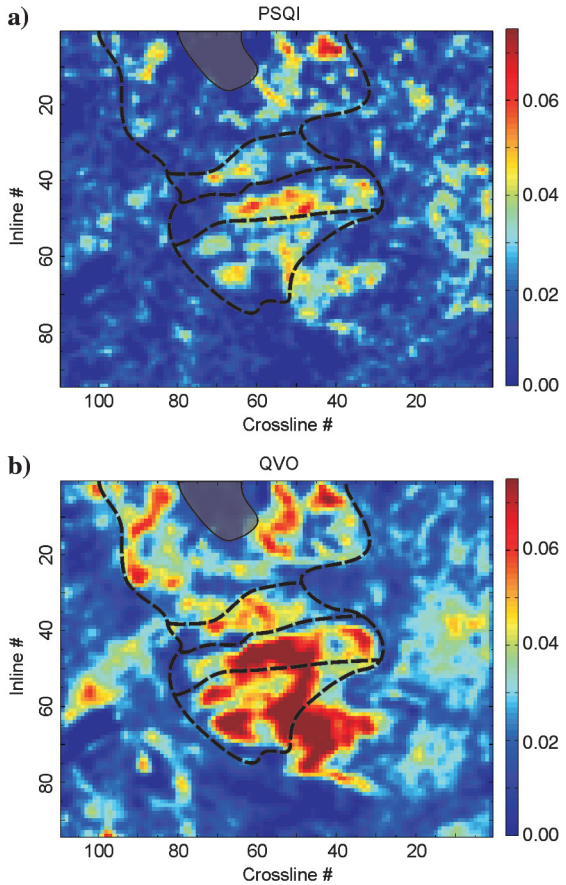

Figure 8. The maps of interval $1/Q$ for the Clearwater to McMurray zone as determined by (a) the PSQI method, and (b) the QVO method. Although the intrinsic attenuation in the zone is expected to be fairly constant, there is a high apparent-attenuation region in the center of the survey. This corresponds to the tuning caused by the high amplitude top-gas reflection (Figure 5), whose identifying boundary is shown. The magnitude of the apparent attenuation effect is reduced for the PSQI measurements. The color bar is clipped below zero, and the lake is grayed out.

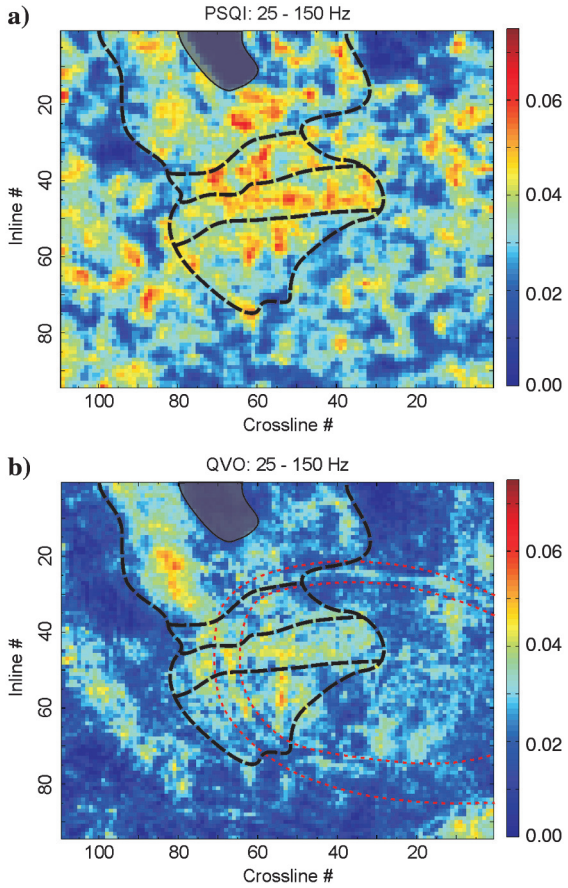

Figure 9. The maps of interval $1/Q$ for the Clearwater to Devonian zone using the primary bandwidth as determined by (a) the PSQI method, and (b) the QVO method. The boundaries and features identified on the amplitude response map (Figure 5) are shown here in black, and correspond well with the higher attenuation features. Measurement errors in the QVO method are compounded by the isochron values (Figure 10), which leave a distinct footprint as outlined in red. The color bar is clipped below zero, and the lake is grayed out.

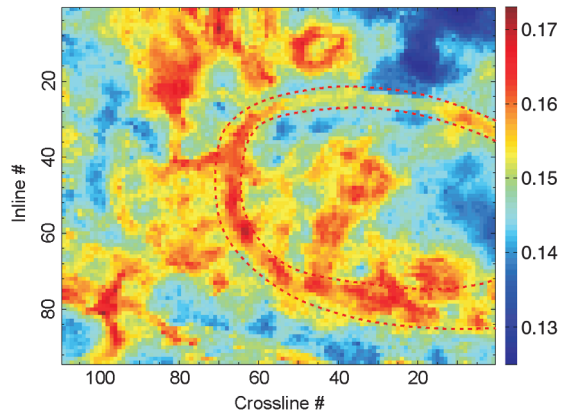

Figure 10. Isochron values between the Clearwater and Devonian horizons, corresponding to the top and base of the measurement interval. These values have a strong influence on the interval $1/Q$ measurements derived from QVO, which unlike PSQI, does not calculate interval values directly. A thick zone, likely an erosional channel, that influences the QVO interval calculations is outlined in a red dashed line.

much, over the original bandwidth measurements (Figure 12c and 12d). These results are summarized in Table 1.

The ability of the PSQI method to deliver meaningful $1/Q$ values is a critical consideration. In this regard, it is significant that the $1/Q$ calculations for the Clearwater to Devonian interval show spatially coherent patterns (Figure 9). This would be expected if the changes in attenuation are due to geological or petrophysical changes in the reservoir, as opposed to random fluctuations in the measurements. Furthermore, the percentage of negative $1/Q$ values across the survey is small (1.4%, dropping to 0.3% when the area of poor data quality beneath the lake is excluded) indicating that the results are not dominated by negative apparent attenuation due to interference effects.

The results of the PSQI analysis also compare favorably to the amplitude response at the top of the reservoir, which is an indicator of the presence of top gas. At the center of the survey, both the attenuation and extracted amplitudes are high, but more significant is the similarity of the boundaries of these regions. Some degree of positional variation is expected, because the amplitude map is derived at the top of the reservoir, whereas the attenuation is measured over a larger interval that bounds it. Nevertheless, the measurements have a normalized coefficient of 2D correlation of −0.77, indicating a strong relationship between the two measurements. The correlation is negative because the amplitudes are negative, whereas the attenuation is positive.

Finally, the distribution of the weighted PSQI $1/Q$ measurements can be used to compare with the measurements from the VSP data. Figure 13 shows this distribution plotted with $1/Q$ obtained from both inversions of the VSP data. Both measurements from the VSP, using a single trace pair and a simultaneous inversion of all trace pairs, fall near the center of the PSQI distribution. In fact, the VSP

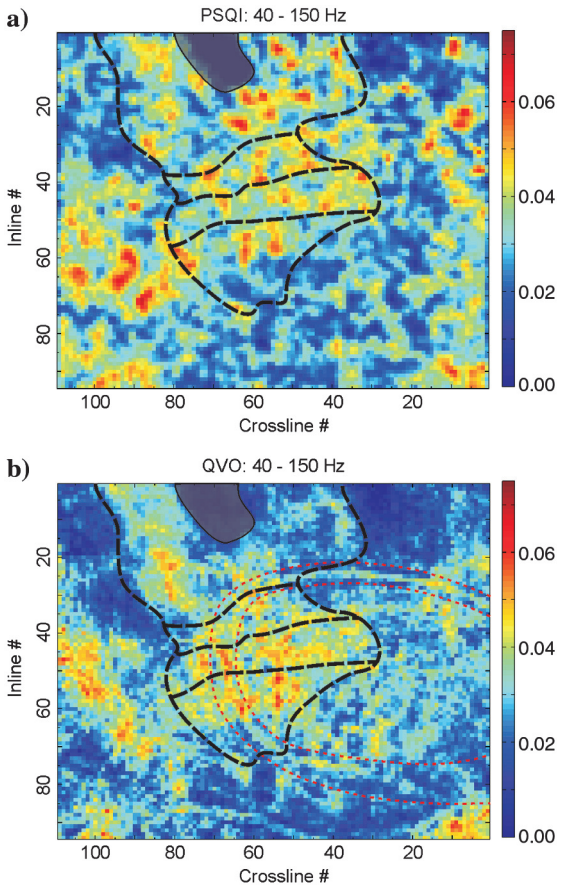

Figure 11. The maps of interval $1/Q$ for the Clearwater to Devonian zone using the bandwidth of 40 to 150 Hz. Both (a) PSQI results, and (b) QVO results are shown. The boundaries and features identified on the amplitude response map (Figure 5) are indicated in black, and the isochron footprint on the QVO map is outlined in red. The QVO measurements show a much larger change from the use of the primary bandwidth (Figure 9) than do the PSQI measurements. The color bar is clipped below zero, and the lake is grayed out.

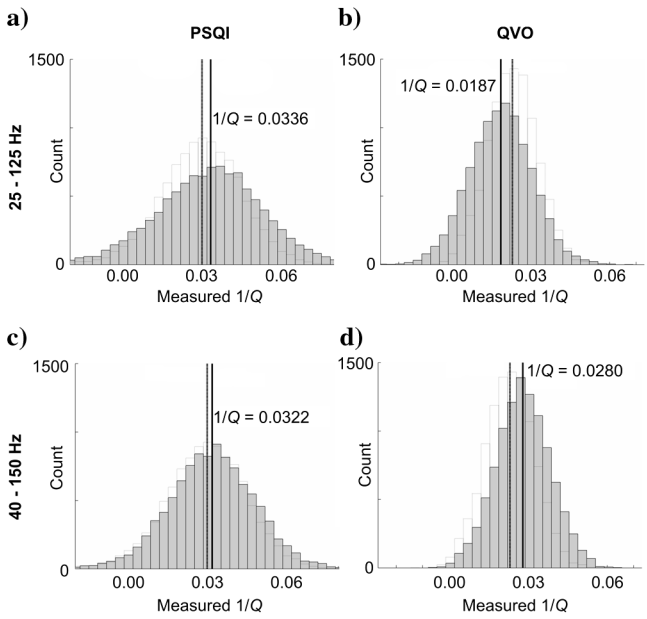

Figure 12. Histograms of the $1/Q$ values calculated over the 3D survey showing the effects of changing the analysis bandwidth. The distributions from the original bandwidth (25 to 150 Hz) are shown as open bars, along with the median values of $1/Q = 0.0303$ for PSQI and $1/Q = 0.0231$ for QVO (dotted vertical lines). (a) The PSQI measurements shift by 0.0033 when the bandwidth is changed to 25 to 125 Hz, compared to (b) the QVO measurements, which shift by −0.0044 for the same bandwidth change. Similarly, (c) the PSQI values shift by 0.0019 when a bandwidth of 40 to 150 Hz is used, compared to (d) a shift of 0.0049 for the QVO values of the same bandwidth change. In both cases, the PSQI results show more stability.

Table 1. Summary of median $1/Q$ results for the Clearwater to Devonian interval over the investigated area using the PSQI and QVO methods. When the inversion bandwidth is changed, the PSQI distribution shows a much smaller shift than that of the QVO measurements. The VSP measurements are also included for comparison, using all pairs simultaneously * and a single receiver-pair **.

Bandwidth	PSQI	QVO	VSP
25–150 Hz	0.0303	0.0231	0.0271* 0.033**
25–125 Hz	0.0336	0.0187	-
40–150 Hz	0.0322	0.0280	-

measurements are less than 0.4σ ($\sigma = 0.0114$) away from the mean PSQI value of $1/Q = 0.0312$.

DISCUSSION

Without a direct confirmation of the actual attenuation values in the reservoir, it is difficult to quantify the accuracy of attenuation measurements using real data. Nevertheless, there are indicators that the results of the PSQI method are appropriate, and that it offers improved reliability over existing methodology. The accuracy of the method using synthetic data was demonstrated in part one of this paper.

The comparison of amplitude and attenuation is a strong piece of supporting evidence of the validity of the measurements. A 77% correlation between these measurements implies that it is statistically likely that they are related, and indeed both amplitude and attenuation effects are explained by the presence of top gas in the reservoir. With respect to the amplitudes, the presence of top gas in the reservoir decreases the impedance and results in a strong negative reflection. Top gas affects attenuation by forming a weaker matrix than one fully saturated (and cemented) by bitumen. Additionally, the increased free space caused by the presence of gas allows for an increase in seismic induced fluid-flow. Both of these factors would increase the attenuation experienced in intervals where gas is present, and this response is seen in the PSQI measurements.

Under the assumption of a frequency-independent Q, the variation in the results caused by a change in the analysis bandwidth shows that the PSQI method is more stable and robust than the QVO method as a means by which to measure $1/Q$ from surface-seismic data. When the bandwidth of the spectral ratio inversion is changed, both methods see a change in the calculated attenuation. Despite this, the magnitude of change is much larger when using the QVO approach. This is a significant advantage of the PSQI method. Because it is not practical to choose a bandwidth manually for every CMP, it is a useful property of a method to be insensitive to bandwidth choice. The bandwidth variability is also an indication of the uncertainty in the $1/Q$ measurements. Although the inversion process allows uncertainty to be calculated, it is a statistical uncertainty of the model fit, and does not indicate bias in the measurement due to interference effects.

The QVO-derived $1/Q$ map also has corrupting influences related to the isochron between the analyzed horizons. This is a result of the QVO method calculating average values from source to interface rather than interval values. To obtain the interval values, the isochron between the interfaces is used. If $1/Q$ is not sensitive enough to small time changes, then these changes imprint themselves on the calculations. This is evidenced in Figure 9 by the curved feature indicated. This same streak appears in the isochron map of the two reservoir bounding horizons, and is likely a channel-erosion feature. The PSQI method calculates interval values directly, and does not encounter this problem.

Comparison with the VSP measurements suggests that the magnitude of the PSQI values is also reasonable for this geological setting. The simultaneously inverted $1/Q = 0.0271 \pm 0.0002$ is well within the distribution of PSQI-measured values for the survey, and in fact is very close to its mean value. Additional support as to the validity of the PSQI values comes from previous investigations of unconsolidated oil sands reservoirs in the region. Macrides and Kanasewich (1987) use a crosswell seismic experiment, and find a value of $1/Q = 0.037 \pm 0.007$ for the heavy-oil saturated Clearwater formation near Cold Lake Alberta. This value is only half of a standard deviation away from the mean of the PSQI distribution.

The lateral variability of the earth in real data violates the assumption of a 1D medium used for analyzing the data in the τ-p domain. We attempt to compensate for some of these consequences, for example by adjusting moveout curves to the maximum instantaneous amplitude to deal with the deviation of interval moveout times from elliptical behavior. Other consequences are less straight forward. For example, in a laterally variable medium, reflections on a single τ-p trace may not share the exact same ray parameter. This would negate some of the reduction in angle-dependent effects in the overburden, but arguably less than the use of a constant reference event.

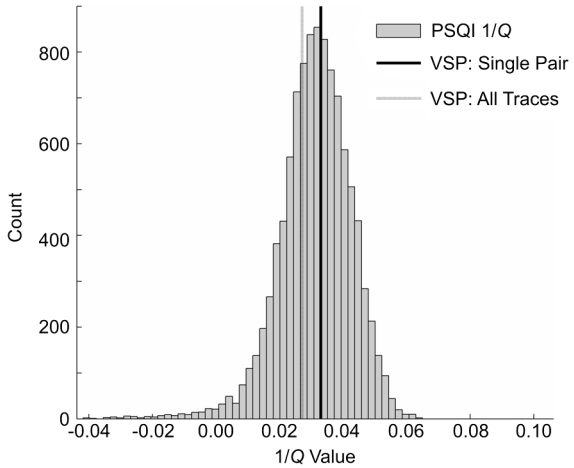

Figure 13. The distribution of the weighted PSQI $1/Q$ results for the investigated area. The VSP $1/Q$ measurements are also shown, both the single trace pair result ($1/Q = 0.033 \pm 0.003$), and the result from using all traces in the simultaneous inversion ($1/Q = 0.0271 \pm 0.0002$). In both instances, the VSP results are very close to the mean PSQI value of $1/Q = 0.0312$.

CONCLUSIONS

In this two-part paper, we have introduced a robust method of measuring attenuation from prestack seismic data. The PSQI method has three main components that set it apart from existing methods: A variable-window time-frequency transform is used to minimize the spectral interference effects caused by tuning and intrabed multiples; an inversion scheme is used that solves for attenuation simultaneously in frequency and traveltime-difference coordinates; and angle-dependent overburden properties are canceled out by analyzing data in the τ-p domain using an assumption of a locally 1D medium.

In part one of this paper, we demonstrated on synthetic data the advantage provided by the PSQI components. In part two, we have shown the validity of the approach on a real 3D data set, demonstrating how the PSQI components fit together into a useful analysis tool. Through a number of supporting measurements, we have also demonstrated the robustness of this method.

Comparing the $1/Q$ measurements from an interval bounding the reservoir to the minimum amplitude below the top of the reservoir results in a 77% correlation. This indicates a strong likelihood that the measured $1/Q$ is driven by reservoir changes rather than random

data artifacts. Additionally, attenuation measurements from a VSP in the same geological environment are very similar in magnitude to the PSQI results. These quantities are further supported by other published attenuation measurements. Finally, the improvement in stability over the QVO method, which does not employ our robust components, further supports their use.

ACKNOWLEDGMENTS

This work was carried out as part of a Ph.D. project at the University of Leeds. We would like to thank Nexen Inc. for providing the funding for this research, as well as the seismic data in conjunction with OPTI Canada Inc. Processing software was provided by Landmark Graphics Corporation through the Landmark University Grant Program. The comments of Yaping Zhu and an anonymous reviewer are also appreciated.

REFERENCES

AEUB, 2003, Athabasca Wabiskaw-McMurray regional geological study: Alberta Energy and Utilities Board.

Behura, J., M. Batzle, R. Hofmann, and J. Dorgan, 2007, Heavy oils: Their shear story: Geophysics, **72**, no. 5, E175–E183, doi: 10.1190/1.2756600.

Blanchard, T. D., R. A. Clark, M. van der Baan, and E. Laws, 2009, Time-lapse attenuation as a tool for monitoring pore fluid changes in hydrocarbon reservoirs: 71st Conference and Exhibition, EAGE, Expanded Abstracts, P052.

Carter, A. J., 2003, Seismic wave attenuation from surface seismic reflection surveys — An exploration tool?: Ph.D. thesis, University of Leeds.

Clark, R. A., P. M. Benson, A. J. Carter, and C. A. Guerrero Moreno, 2009, Anisotropic P-wave attenuation measured from a multi-azimuth surface seismic reflection survey: Geophysical Prospecting, **57**, 835–845, doi: 10.1111/gpr.2009.57.issue-5.

Clark, R. A., A. J. Carter, P. C. Nevill, and P. M. Benson, 2001, Attenuation measurements from surface seismic data — Azimuthal variation and time-lapse case studies: 63rd Conference and Technical Exhibition, EAGE, Extended Abstracts, L–28.

Dasgupta, R., and R. A. Clark, 1998, Estimation of Q from surface seismic reflection data: Geophysics, **63**, 2120–2128, doi: 10.1190/1.1444505.

Dix, C. H., 1955, Seismic velocities from surface measurements: Geophysics, **20**, 68–86, doi: 10.1190/1.1438126.

Guerrero Moreno, C. A., 2007, Fracture induced seismic wavespeed and attenuation anisotropy in hydrocarbon exploration: Ph.D. thesis, University of Leeds.

Hackert, C. L., and J. O. Parra, 2004, Improving Q estimates from seismic reflection data using well-log-based localized spectral correction: Geophysics, **69**, 1521–1529, doi: 10.1190/1.1836825.

Macrides, C. G., and E. R. Kanasewich, 1987, Seismic attenuation and poisson's ratios in oil sands from crosshole measurements: Canadian Journal of Exploration Geophysics, **23**, 46–55.

Moffat, L. C., R. A. Clark, M. van der Baan, and T. Manning, 2009, Azimuthal variations of attenuation analysis applied on a 3D multi-azimuth towed-streamer dataset: Research Workshop, EAGE/SEG, Expanded Abstracts, B06.

Reine, C., 2009, A robust prestack Q-inversion in the τ-p domain using variable window spectral estimates: Ph.D. thesis University of Leeds.

Reine, C., M. van der Baan, and R. Clark, 2009, The robustness of seismic attenuation measurements using fixed- and variable-window time-frequency transforms: Geophysics, **74**, no. 2, WA123–WA135, doi: 10.1190/1.3043726.

Stockwell, R. G., L. Mansinha, and R. P. Lowe, 1996, Localization of the complex spectrum: The S transform: IEEE Transactions on Signal Processing, **44**, 998–1001, doi: 10.1109/78.492555.

Taner, M. T., and F. Koehler, 1981, Surface consistent corrections: Geophysics, **46**, 17–22, doi: 10.1190/1.1441133.

Taner, M. T., F. Koehler, and R. E. Sheriff, 1979, Complex seismic trace analysis: Geophysics, **44**, 1041–1063, doi: 10.1190/1.1440994.

Ursin, B., 1990, Offset-dependent geometrical spreading in a layered medium: Geophysics, **55**, 492–496, doi: 10.1190/1.1442860.

van der Baan, M., 2004, Processing of anisotropic data in the τ-p domain: I — Geometric spreading and moveout corrections: Geophysics, **69**, 719–730, doi: 10.1190/1.1759458.

Wang, Y., 2002, A stable and efficient approach of inverse Q filtering: Geophysics, **67**, 657–663, doi: 10.1190/1.1468627.

Wightman, D. M., and S. G. Pemberton, 1997, The lower Cretaceous (Aptian) McMurray formation: An overview of the Fort McMurray area, northeastern, Alberta, *in* S. G. Pemberton, and D. P. James, eds., Petroleum geology of the Cretaceous Mannville group, western Canada: CSPG memoir 18, 312–344.

Winkler, K. W., and A. Nur, 1982, Seismic attenuation: Effects of pore fluids and frictional sliding: Geophysics, **47**, 1–15, doi: 10.1190/1.1441276.